Hindawi Publishing Corporation
International Journal of Photoenergy
Volume 2012, Article ID 265760, 9 pages
doi:10.1155/2012/265760

Research Article

Enhanced Photocatalytic Activity of TiO_2 Powders (P25) via Calcination Treatment

Guohong Wang,[1] Lin Xu,[1] Jun Zhang,[2] Tingting Yin,[1] and Deyan Han[1]

[1] *College of Chemistry and Environmental Engineering, Hubei Normal University, Huangshi, Hubei 435002, China*
[2] *State Key Laboratory of Advanced Technology for Material Synthesis and Processing, Wuhan University of Technology, Luoshi Road 122, Wuhan 430070, China*

Correspondence should be addressed to Guohong Wang, wanggh2003@163.com

Received 14 September 2011; Revised 7 November 2011; Accepted 8 November 2011

Academic Editor: Jiaguo Yu

P25 TiO_2 powders were calcined at different temperatures in a muffle furnace in air. The P25 powders before and after calcination treatment were characterized with XRD FTIR, UV-visible diffuse reflectance spectra, SEM, TEM, HRTEM, and N_2 adsorption-desorption measurements. The photocatalytic activity was evaluated by the photocatalytic oxidation of methyl orange aqueous solution under UV light irradiation in air. The results showed that calcination treatment obviously influenced the microstructures and photocatalytic activity of the P25 TiO_2 powders. The synergistic effect of the phase structure, BET surface area, and crystallinity on the photocatalytic of TiO_2 powders (P25) after calcination was investigated. An optimal calcination temperature (500°C) was determined. The photocatalytic activity of TiO_2 powders calcined at 500°C was nearly 2 times higher than that of the uncalcined P25 TiO_2. The highest photocatalytic activities of the calcined samples at 500°C for 4 h might be ascribed to the enhancement of anatase crystallization and the optimal mass ratio (ca. 1 : 2) of rutile to anatase.

1. Introduction

A number of investigations have focused on the semiconductor photocatalyst for its applications in solar energy conversion and environmental purification since Fujishima and Honda discovered the photocatalytic splitting of water on the TiO_2 electrodes in 1972 [1, 2]. Among various oxide semiconductor photocatalysts, titania has been proven to be the most suitable for widespread environmental applications for its biological and chemical inertness, strong oxidizing power, cost effectiveness, and long-term stability against photo- and chemical corrosion [3–6]. However, the practical applications of TiO_2 are greatly limited due to the wide band-gap (anatase ca. 3.2 eV, rutile ca. 3.0 eV) and the resultant low utilization of solar energy and fast recombination of photogenerated electrons and holes [7–9]. Therefore, the photocatalytic activity of titania must be further enhanced from the point of view of practical use and commerce. Many methods have been developed for enhancing the efficiency of the TiO_2 powders. These include doping with metal and nonmetal elements [10–13], dye sensitization [14, 15], and semiconductor coupling [16, 17], and so forth.

It is wellknown that the photocatalytic activity of TiO_2 system mainly depends on its intrinsic properties, such as phase structures, specific surface area, crystallinity, and preparing methods [18]. For example, many studies have confirmed that the anatase phase of titania is a good photocatalytic material due to its low recombination rate of photogenerated electrons and holes [19, 20]. In our previous observations, it was found that the composite of two phases of titania was more beneficial for suppressing the recombination of photogenerated electrons and holes and thus enhanced the photocatalytic activity [21]. In addition, a posttreatment condition is also another important factor that influences the photocatalytic activity of TiO_2 powders. Usually, two principle posttreatment methods have been used to control the physicochemical properties of the TiO_2 powders. One is hydrothermal treatment. Yu et al. [22] demonstrated an obvious increase of photocatalytic activity after hydrothermal treatment of TiO_2 (P25) and thought that the increase in photoactivity can be attributed to the formation of more hydroxyl groups in the surface of TiO_2. Another method is calcination after treatment. By changing the calcination conditions, such as calcination temperatures,

calcination time, and heating rate crystalline products with different compositions, structures, and morphologies have been obtained. Yu et al. suggested that thermal treatment could allow more oxygen molecules to be adsorbed on the surface of TiO_2 [23]. Sato et al. and Zhang et al. thought that an enhancement in photocatalytic activity was ascribed to the fact that the calcination released lattice oxygen from TiO_2 [24, 25]. However, to the best of our knowledge, few studies have been carried out on the synergistic effect of the phase structure, BET surface area, and crystallinity on the photocatalytic of TiO_2 powders (P25) after calcination. In the present work, we prepared highly active TiO_2 powder photocatalyst via calcination after treatment of Degussa P25. The photocatalytic activity of the as-prepared TiO_2 powders was evaluated by the photocatalytic oxidation of methyl orange aqueous solution under UV light irradiation in air. The reasons for the enhanced photocatalytic activity of the calcinations-treated TiO_2 samples were discussed.

2. Experimental Section

2.1. Sample Preparation. Commercial Degussa P25 TiO_2 was used as supplied. In a typical calcination process, 1.0 g of P25 powder was transferred into a 30 mL crucible, followed by calcination at 400–800°C in a muffle furnace for 4 h. After the thermal treatment, the crucible containing catalysts was cooled to room temperature to obtain the as-synthesized TiO_2 powders. The calcined P25 and untreated Degussa P25 samples were characterized for evaluating the changes in properties.

2.2. Characterization. The X-ray diffraction (XRD) patterns obtained on an X-ray diffractometer (type D8 ADVANCE) using Cu-Kα irradiation at a scan rate (2θ) of $0.02^\circ\,s^{-1}$ were used to determine the identity of any phase present and their crystallite size. The accelerating voltage and the applied current were 15 kV and 20 mA, respectively. If the sample contains anatase and rutile phases, the phase content of titania can be calculated from the integrated intensities of anatase (101) and rutile (110) peaks, according to the following equation [22]:

$$f_R = \frac{1.26\, I_R}{I_A + 1.26\, I_R}, \quad (1)$$

where I_A and I_R represent the integrated intensity of the anatase (101) and rutile (110) peaks, respectively. With (1), the phase contents of anatase and rutile in TiO_2 samples can be calculated. The average crystallite sizes of anatase and rutile were determined according to the Scherrer equation. Crystallite sizes and shapes were observed using transmission electron microscopy (TEM) and high-resolution transmission electron microscopy (HRTEM) (JEOL-2010F at 200 kV). The samples for TEM observation were prepared by dispersing the TiO_2 powders in an absolute ethanol solution under ultrasonic irradiation; the dispersion was then dropped on carbon-copper grids. The Brunauer-Emmett-Teller surface area (S_{BET}) of the powders was analyzed by nitrogen adsorption in a Micromeritics ASAP 2020 nitrogen adsorption apparatus (USA). All the samples were degassed at 180°C prior to nitrogen adsorption measurements. The BET surface area was determined by multipoint BET method using the adsorption data in the relative pressure (P/P_0) range of 0.05–0.3. Desorption isotherm was used to determine the pore-size distribution via the Barret-Joyner-Halender (BJH) method, assuming a cylindrical pore modal [26–28]. The nitrogen adsorption volume at the relative pressure (P/P_0) of 0.994 was used to determine the pore volume and average pore size. The morphologies of TiO_2 powders were observed using scanning electron microscopy (SEM) (type JSM-7001F, Japan) with an acceleration voltage of 20 kV. The UV-Vis spectra were obtained by an UV-Vis spectrophotometer (UV-2550, Shimadzu, Japan). Infrared (IR) spectra on pellets of the samples mixed with KBr were recorded on a Nicolet 5700 FTIR spectrometer at a resolution of $0.09\,cm^{-1}$. The concentration of the samples was kept at about 0.25–0.3%.

2.3. Measurement of Photocatalytic Activity. The photocatalytic activity evaluation of TiO_2 powders for the photocatalytic decolorization of methyl orange aqueous solution was performed at ambient temperature. The detailed experimental process can be found in our previous studies [5]. The photocatalytic decolorization of methyl orange aqueous solution is a pseudo-first-order reaction and its kinetics may be expressed as $\ln(c_0/c) = kt$, where k is the apparent rate constant, and c_0 and c are the adsorption-desorption equilibrium and reaction concentrations of aqueous methyl orange, respectively.

3. Results and Discussion

3.1. Phase Structure. The effect of calcination temperature on phase structures was studied using XRD. Figure 1 shows the XRD patterns of P25 powders before and after calcination at different temperatures for 4 h. It can be seen that all the samples were composed of both rutile and anatase phases. Further observation shows that with increasing calcination temperature form 400 to 500°C, the intensity of both anatase and rutile peaks gradually increases, indicating an enhancement of crystallization. With further increasing temperature from 600 to 800°C, the intensities of anatase diffraction peaks decreased gradually and ultimately disappeared, and meanwhile the intensities of rutile diffraction peaks steadily became stronger. Therefore, the calcination temperature obviously influences the crystallization and phase composition of the P25 powders. The effects of calcination temperatures on physical properties of P25 TiO_2 powders are shown in Table 1. It can be seen that the mass fraction of rutile phase slightly increases with increasing calcination temperature. Before calcination, the mass fraction of rutile was ca. 27.3%. At 700°C, the content of rutile reached ca. 90.8%. No anatase phase was detected at 800°C, which is in good agreement with results in the literature [29]. Therefore, it is reasonable to suggest that high calcination temperature results in the phase transformation from anatase to rutile. Usually, phase transformation is accompanied with crystal growth.

Table 1: Effect of temperature on physicochemical properties of TiO_2 samples.

Temperature (°C)	[a]Phase content (%)	[b]Crystalline size (nm)	[c]S_{BET} (m^2/g)	[d]Pore volume (cm^3/g)	Average pore size (nm)	[e]Porosity (%)
P25	A: 72.7; R: 27.3	29.5	45.7	0.177	7.57	41.5
400	A: 72.7; R: 27.3	31.7	25.9	0.0929	8.24	27.1
500	A: 66.4; R: 33.6	33.8	22.7	0.0597	10.7	19.4
600	A: 55.2; R: 44.8	48.6	18.7	0.0503	10.5	17.0
700	A: 9.8; R: 90.2	63.2	8.59	0.0177	14.4	7.00
800	R: 100	99.0	4.39	0.00831	15.5	3.45

Calcination time: 4 h

[a]A and R denote anatase and rutile, respectively. [b]Average crystalline size of TiO_2 was determined by XRD using Scherrer equation. [c]The BET surface area was determined by multipoint BET method using the adsorption data in P/P_0 range from 0.05 to 0.3. [d]Pore volume and average pore size were determined by nitrogen adsorption volume at $P/P_0 = 0.994$. [e]The porosity is estimated from the pore volume determined using the desorption data at $P/P_0 = 0.994$.

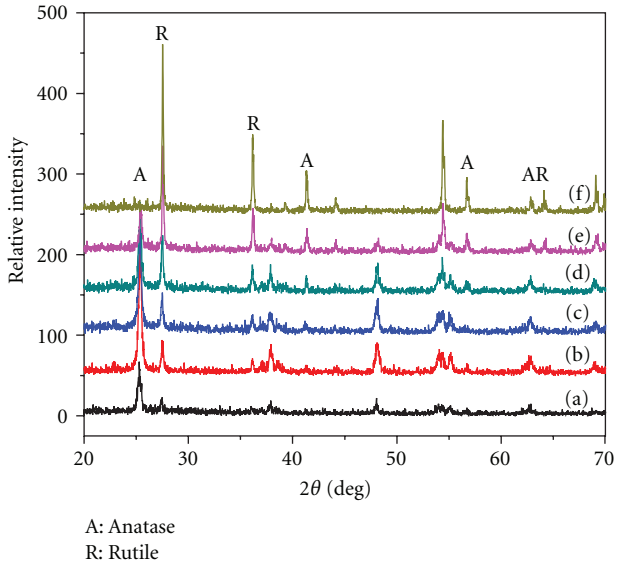

Figure 1: XRD patterns of P25 samples before (a) and after calcination at 400 (b), 500 (c), 600 (d), 700 (e), and 800°C (f) for 4 h.

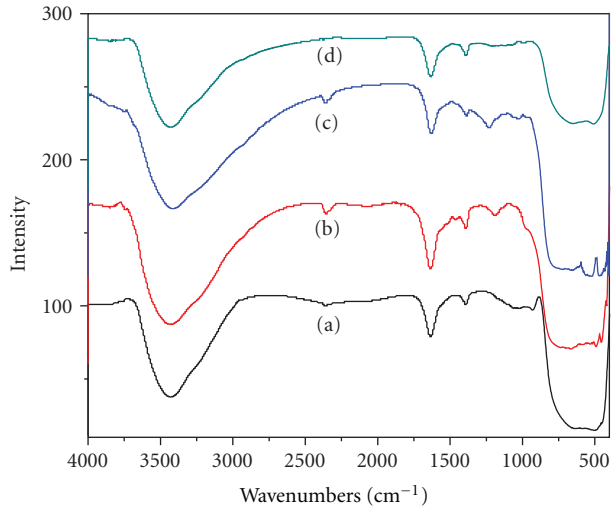

Figure 2: FT-IR spectra of the P25 powders before (a) and after calcination at 400 (b), 500 (c), and 600°C (d) for 4 h.

As the calcination temperature is raised, XRD reflections corresponding to both the anatase and rutile phase become narrower, which indicates the increase of crystallite size. The average crystallite size was shown in Table 1. The average crystallite size of samples treated at lower temperature (below 500°C) increased slightly from about 29.5 to 33.8 nm (see Table 1). However, higher temperature caused rapid increase of crystallite size up to about 63.2 and 99 nm for samples calcined at 700 and 800°C, respectively. The similar results were observed by Górska et al. [30] for five different samples of TiO_2 calcinated at 400–750°C.

3.2. FT-IR. The preparation methods and conditions could affect the hydroxylation state of titania powders. The FT-IR spectroscopy of the P25 before and after calcination treatment of 4 h is shown in Figure 2. It is believed that the broad peak at 3400 and the peak at 1650 cm^{-1} correspond to the surface-adsorbed water and hydroxyl groups, respectively. The main peak at 400–700 cm^{-1} was attributed to Ti-O stretching and Ti-O-Ti bridging stretching modes [31]. Notably, with increasing temperature, the surface-adsorbed water and hydroxyl groups decreased slightly. This was due to the decrease of specific surface areas and pore volume (as shown in Table 1), which caused the reduction of the adsorbed water [32]. According to our previous study, the hydroxyl groups on the surface of samples contribute to enhancement of the photocatalytic activity [33], because they can interact with photogenerated holes, which gives better charge transfer and inhibits the recombination of electron-hole pairs [34, 35].

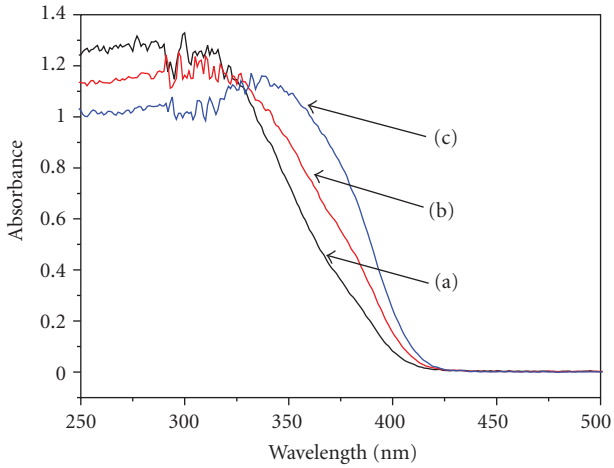

Figure 3: UV-Vis absorption spectra of P25 powders before (a) and after calcination at 500 (b), and 700°C (c) for 4 h.

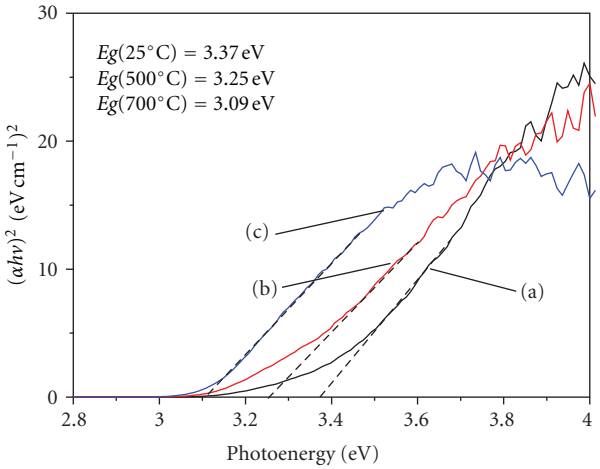

Figure 4: Plots of $(h\nu\alpha)^2$ versus photon energy for the P25 powders before (a) and after calcination at 500 (b), and 700°C (c) for 4 h.

3.3. UV-Vis Spectra. Usually, calcination temperature obviously affects light absorption characteristics of TiO_2 [36–38]. The influences of temperature on the light absorption characteristics of TiO_2 powders are shown in Figure 3. A significant increase at wavelengths shorter than 420 nm could be attributed to absorption of light caused by the excitation of electrons from the valence band to the conduction band of TiO_2. A red shift of the absorbance spectra of TiO_2 powders calcined at 500 and 700°C in the band gap transition was observed as compared with the uncalcined P25 powders. The differences in adsorption were attributed to the change of crystallite size and phase structure (see Table 1).

The adsorption edges shifted toward longer wavelengths for the powders after calcination at 500 and 700°C. This clearly indicated a decrease in the band gap energy of TiO_2. To further explore the effect of calcination temperature on the absorption edge, the band gap energy can be estimated from a plot of $(h\nu\alpha)^{1/2}$ versus photon energy $(h\nu)$. The intercept of the tangent to the plot will give a good approximation of the indirect band gap energy for TiO_2. The relation

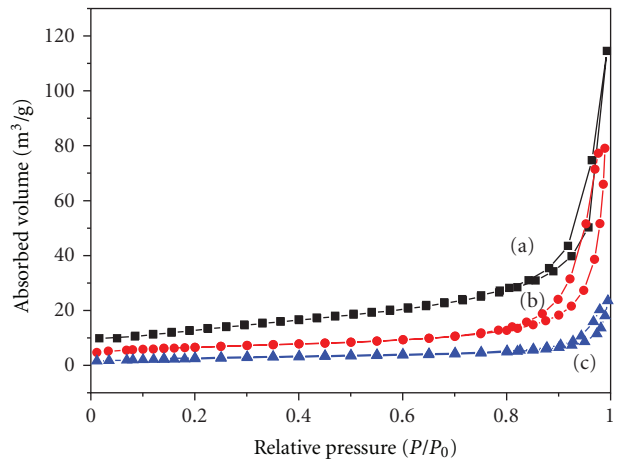

Figure 5: Nitrogen adsorption-desorption isotherms of the P25 powders before (a) and after calcination at 500 (b) and 700°C (c) for 4 h.

between the absorption coefficient (α) and incident photon energy $(h\nu)$ can be written as $\alpha = B_i(h\nu - Eg)^{1/2}/h\nu$, where B_i is absorption constants for indirect transitions [39–41]. Since absorbance (A) is proportional to absorption coefficient (α), we use absorbance (A) to substitute absorption coefficient (α) [40].

Plots of $(h\nu\alpha)^2$ versus photon energy $(h\nu)$ for TiO_2 powders are shown in Figure 4. The band gap energies estimated from the intercept of the tangents of the plots are 3.37, 3.25, and 3.10 eV for the P25 powders before and after calcination at 500 and 700°C for 4 h, respectively. This showed that the band gap of TiO_2 samples monotonically became narrower with increasing calcinations temperatures. This may be due to the following factors: (1) an increase in the crystallite size resulted in the decrease of band gap energy, which was in accordance with previous results reported by Xiao et al. [42]; (2) lower value of band gap for samples after calcination at 500 and 700°C may be a result of phase transformation from anatase to rutile [30].

3.4. BET Surface Areas and Pore Distribution. Figure 5 shows nitrogen adsorption-desorption isotherms of the P25 powders before and after calcination at 500 and 700°C. It can be seen that all the samples show a type H3 hysteresis according to BDDT classification [26], indicating the presence of mesopores (2–50 nm). Moreover, the observed hysteresis approaches to $P/P_0 = 1$, suggesting the presence of large pores (>50 nm) [43, 44]. Further observation indicates that with increasing calcination temperature, the hysteresis loops shift to higher relative pressure range and the areas of the hysteresis loops decrease. This indicated that the average pore size increased and the volume of pore decreased with increasing calcination temperatures [45]. When the calcination temperature is higher than 700°C, the hysteresis loops of the obtained samples are difficult to be observed (not shown in Figure 5), indicating that some pores collapse during the calcination. The pore size distribution calculated from the desorption branch of the isotherm is presented

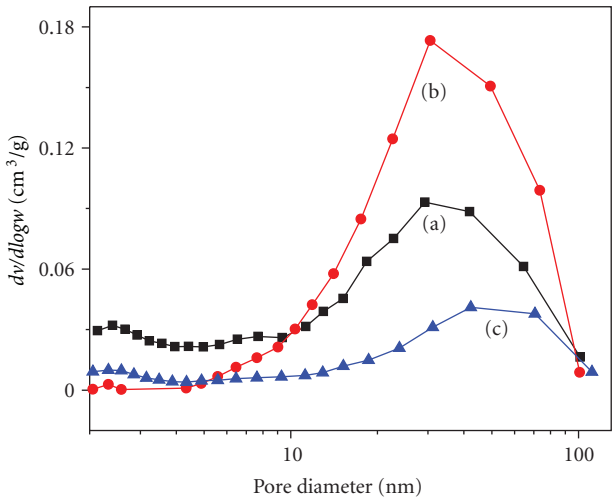

Figure 6: Pore diameter distribution curves of the P25 powders before (a) and after calcination at 500 (b) and 700°C (c) for 4 h.

in Figure 6. It can be seen that calcination temperature significantly influences the pore size distribution of the TiO_2 powders. Before calcination, the P25 TiO_2 has a wide pore size distribution from mesopore to macropore. With increasing calcination temperatures, the curves of the pore size distribution shift to the macropore region and the pore volumes decrease slowly. At 700°C, the pore size distribution becomes even, indicating the disappearance of pores [6]. Usually, the average pore size is connected with the TiO_2 crystallite size and the average pore size increased with an increase in the crystallite size of TiO_2 powders [21, 22, 46, 47]. Accordingly, the decrease of pore volume located at 2–10 nm for the calcined P25 powders indicated the decrease of smaller TiO_2 crystallites (<10 nm). This is in good agreement with the XRD analysis in which smaller anatase crystallites were transformed into rutile phase. Table 1 shows the physical properties of the P25 powders before and after calcination treatment at different temperatures for 4 h. Before calcination treatment, P25 TiO_2 shows a large BET-specific surface area, and its value reaches 45.7 m^2/g. After calcination treatment above 400°C, the BET-specific surface areas of the P25 samples clearly decrease. Further observation shows that with increasing calcination temperatures, the BET-specific surface areas, pore volumes, and porosity steadily decrease; meantime, the average pore size increases.

3.5. SEM and TEM. The calcination process also affects the morphologies of the resulting P25 TiO_2 powders. Figure 7 shows SEM images of the P25 TiO_2 powders before and after calcination treatment at 400, 500, and 700°C for 4 h. It can be seen from Figure 7(a) that before calcination treatment, the powders are smaller aggregated particles, resulting in a high porous volume due to aggregation among tiny TiO_2 particles (see Figure 6). Conversely, after calcination treatment, the powders are composed of larger agglomerated particles. This may be caused by the phase transformation from anatase to rutile, resulting in the decrease in the pore volume (as shown in Table 1). It is interesting to observe from Figure 7 that with increasing calcination temperature from 400 to 700°C, the particle sizes of the aggregates gradually increase. This may be ascribed to the fact that the interaction of smaller particles results in their aggregation into many spherical particles with bigger sizes. The morphology and microstructures of P25 TiO_2 powders are further investigated by TEM and HRTEM analysis. Figure 8(a) shows a typical TEM image of the TiO_2 powders after calcination at 500°C for 4 h. It can be seen that the particles exhibit a relatively uniform particle size distribution. The average size of the primary particles estimated from the TEM image is about 35 nm, which is in good agreement with that calculated from the XRD pattern using Scherrer equation (33.8 nm). Further observation indicates that a large number of mesopores come from the aggregation of primary particles or crystallites. Figure 8(b) presents a typical HRTEM lattice image of the TiO_2 nanoparticles after calcination at 500°C for 4 h. The selected area electron diffraction (SAED) patterns (inset in Figure 8(b)) reveal the polycrystalline nature of the anatase and rutile phases for the P25 TiO_2 powders. By measuring the lattice fringes, the resolved interplanar distances are ca. 0.35 and 0.33 nm, corresponding to the (101) planes of anatase and the (110) planes of rutile, respectively. This further confirms the mixed biphase structures of the sample after calcination at 500°C for 4 h.

3.6. Photocatalytic Activity. The photocatalytic activity of the P25 TiO_2 before and after calcination at various temperatures was evaluated by photocatalytic oxidation of methyl orange (MO) aqueous solution under UV light irradiation in air. Figure 9 shows the relationship between the apparent rate constants (k) of MO degradation and calcination temperatures. Prior to calcination, the P25 TiO_2 showed high photocatalytic activity with a rate constant of 6.02×10^{-3}, which is a well known and recognized as an excellent photocatalyst. It has been reported that the P25 TiO_2 photocatalyst are consists of an amorphous state together with a mixture of anatase and rutile [48]. Further observation indicates that the calcined sample at 400°C for 4 h shows a higher photocatalytic activity with a rate constant of 10.2×10^{-3}. This may be due to the fact calcination treatment enhanced the phase transformation of the P25 TiO_2 powders from amorphous to anatase. The rate constants increase with increasing calcination temperatures. The enhancement of photocatalytic activity at elevated calcination temperatures can be ascribed to an obvious improvement in anatase crystallinity (as shown in Figure 1). At 500°C, the k reaches the highest value of 12.1×10^{-3}. With further increasing the calcination temperature, the k decreases slightly. This is due to the decrease in specific surface areas and the content of anatase (as shown in Table 1). The highest photocatalytic activities of the calcined samples at 500°C might be explained by the optimal mass ratio of rutile to anatase.

Generally, photocatalytic activity of mesoporous TiO_2 is strongly dependent on its phase structure, crystallite size, surface areas, and pore structure. Larger specific surface area allows more organic reactants to be absorbed onto the surface of the photocatalyst, while higher pore volume results

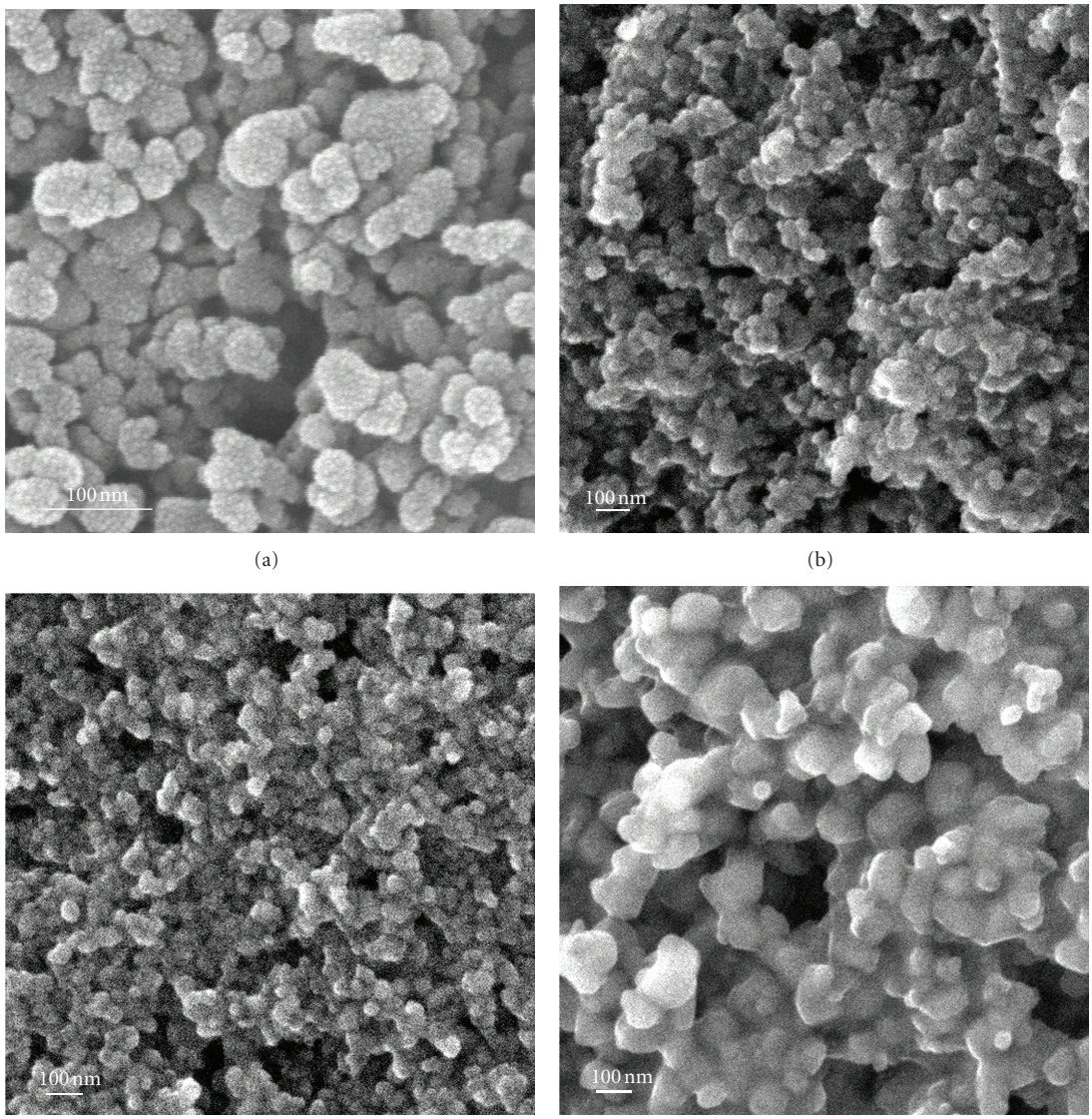

Figure 7: SEM images of the P25 powders before (a) and after calcined at 400 (b), 500 (c), and 700°C (d) for 4 h.

in a rapider diffusion of various inorganic products during the photocatalytic reaction. Therefore, it is expected that the uncalcined sample exhibits a relative high photocatalytic activity due to its large specific surface areas and pore volume. However, the powders with a large surface area are usually associated with large amounts of crystalline defects or weak crystallization, which favor the recombination of photogenerated electrons and holes, leading to a poor photoactivity. Therefore, the large surface area is a requirement, but not a decisive factor. It is well known that the mixture of anatase and rutile TiO_2 has higher degradation efficiency than pure anatase for the oxidation of various organic compounds [48–50]. Moreover, the content of rutile has played important role in photocatalytic reaction. For example, Bacsa et al. found that the catalyst with 30% rutile content showed a maximum catalytic activity for the photocatalyzed degradation of *p*-coumaric acid [51]. It was reported the TiO_2 powders containing 77% anatase and 23% rutile had highest photocatalytic activity in degradation of 4-chlorophenol [52]. Thus, the mass ratio of rutile to anatase is another important factor that influences the photocatalytic efficiency [53, 54]. In our present work, the uncalcined P25 powders possess a large specific surface area of 45.7 m^2/g. After calcination at 500°C, the specific surface areas decrease to 22.7 m^2/g. Such a large decrease in specific surface area should lead to a decrease in the photocatalytic activity. However, the 500°C sample shows the highest photocatalytic activity. The increase of photocatalytic activity at 500°C might be due to the enhancement of anatase crystallization and increase of rutile content in photocatalysts (as shown in Figure 1 and Table 1). The former is beneficial to reduce the recombination rate of the photogenerated electrons and

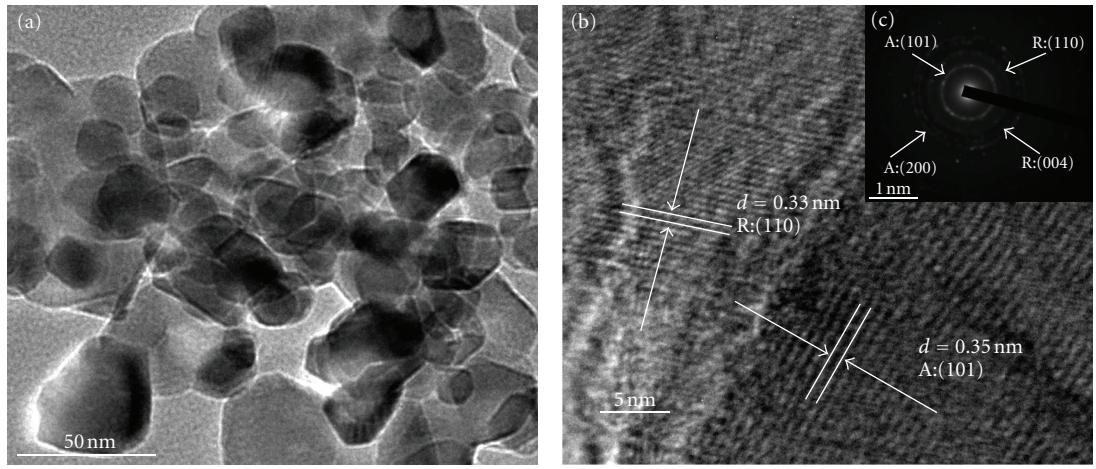

(a) (b)

Figure 8: TEM (a) and HRTEM (b) images and SAED pattern (inset in (b)) of the TiO_2 samples calcined at 500°C for 4 h.

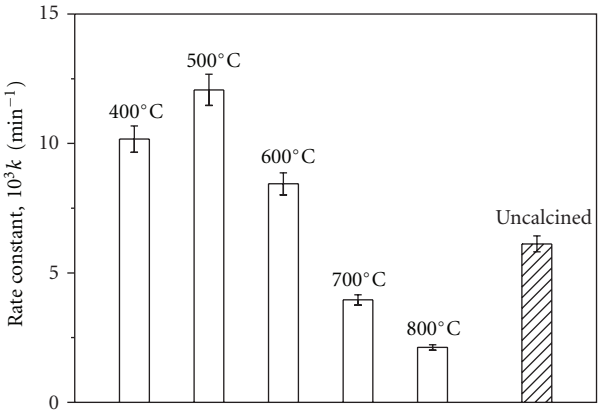

Figure 9: Effects of calcination temperatures on the apparent rate constants of the P25 powders.

holes due to the decrease in number of the defects. The latter can enhance the transfer and separation of photogenerated electrons and holes, implying that the mass ratio of rutile to anatase also obviously influences photocatalytic activity and an optimal rutile-to-anatase mass ratio is probably ca. 1 : 2 according to our results. According to the aformentioned deduction, it is not difficult to explain that the 700 and 800°C samples show a lower photocatalytic activity than the 500°C sample due to the increase of rutile content in photocatalysts.

4. Conclusion

Calcination treatment exhibits a marked influence on the microstructures and photocatalytic activity of the P25 TiO_2 powders. With increasing calcination temperature, the average crystallite size, average pore size, and rutile content increase. In contrast, the BET-specific surface areas, pore volumes, and porosity steadily decrease. The synergistic effect of the phase structure, BET surface area, and crystallinity on the photocatalytic of TiO_2 powders (P25) after calcination was investigated. An optimal calcination temperature (500°C) was determined. The photocatalytic activity of TiO_2 powders at an optimal calcination temperature was nearly 2 times higher than that of the uncalcined P25 TiO_2. The highest photocatalytic activities of the calcined samples at 500°C for 4 h might be ascribed to the enhancement of anatase crystallization and the optimal mass ratio (ca. 1 : 2) of rutile to anatase.

Acknowledgments

This work was partially supported by NSFC (21075030, 51072154, and 51102190) and the Mid-young Scholars' Science and Technology Programs, Hubei Provincial Department of Education (Q20082202).

References

[1] A. Fujishima and K. Honda, "Electrochemical photolysis of water at a semiconductor electrode," *Nature*, vol. 238, no. 5358, pp. 37–38, 1972.

[2] S. W. Liu, J. G. Yu, and M. Jaroniec, "Anatase TiO_2 with dominant high-energy {001} facets: synthesis, properties, and applications," *Chemistry of Materials*, vol. 23, no. 18, pp. 4085–4093, 2011.

[3] A. Yu, G. Q. M. Lu, J. Drennan, and I. R. Gentle, "Tubular titania nanostructures via layer-by-layer self-assembly," *Advanced Functional Materials*, vol. 17, no. 14, pp. 2600–2605, 2007.

[4] Q. J. Xiang, J. G. Yu, and P. K. Wong, "Quantitative characterization of hydroxyl radicals produced by various photocatalysts," *Journal of Colloid and Interface Science*, vol. 357, no. 1, pp. 163–167, 2011.

[5] J. G. Yu, H. G. Yu, B. Cheng, X. J. Zhao, J. C. Yu, and W. K. Ho, "The effect of calcination temperature on the surface microstructure and photocatalytic activity of TiO_2 thin films prepared by liquid phase deposition," *Journal of Physical Chemistry B*, vol. 107, no. 50, pp. 13871–13879, 2003.

[6] J. G. Yu, J. F. Xiong, B. Cheng, and S. W. Liu, "Fabrication and characterization of Ag–TiO_2 multiphase nanocomposite thin

films with enhanced photocatalytic activity," *Applied Catalysis B: Environmental*, vol. 60, no. 3-4, pp. 211–221, 2005.

[7] Y. Z. Fan, G. P. Chen, D. M. Li et al., "Highly slective dethylation of Rdamine B on TiO_2 prepared in supercritical fluids," *International Journal of Photoenergy*, vol. 2012, Article ID 173865, 7 pages, 2012.

[8] N. H. Lee, H. J. Oh, S. C. Jung, W. J. Lee, D. H. Kim, and S. J. Kim, "Photocatalytic properties of nanotubular-shaped TiO_2 powders with anatase phase obtained from titanate nanotube powder through various thermal treatments," *International Journal of Photoenergy*, vol. 2011, Article ID 327821, 7 pages, 2011.

[9] J. A. Byrne, P. A. Fernandez, P. S. M. Dunlop, D. M. A. Alrousan, and J. W. J. Hamilton, "Photocatalytic enhancement for solar disinfection of water: a review," *International Journal of Photoenergy*, vol. 2011, Article ID 798051, 12 pages, 2011.

[10] L. C. Kong, G. T. Duan, G. M. Zuo, W. Cai, and Z. Cheng, "Rattle-type Au@TiO_2 hollow microspheres with multiple nanocores and porous shells and their structurally enhanced catalysis," *Materials Chemistry and Physics*, vol. 123, no. 2-3, pp. 421–426, 2010.

[11] V. Rodríguez-González, S. O. Alfaro, L. M. Torres-Martínez, S. H. Cho, and S. W. Lee, "Silver-TiO_2 nanocomposites: synthesis and harmful algae bloom UV-photoelimination," *Applied Catalysis B: Environmental*, vol. 98, no. 3-4, pp. 229–234, 2010.

[12] L. Ravichandran, K. Selvam, and M. Swaminathan, "Highly efficient activated carbon loaded TiO_2 for photo defluoridation of pentafluorobenzoic acid," *Journal of Molecular Catalysis A: Chemical*, vol. 317, no. 1-2, pp. 89–96, 2010.

[13] J. G. Yu, T. T. Ma, and S. W. Liu, "Enhanced photocatalytic activity of mesoporous TiO_2 aggregates by embedding carbon nanotubes as electron-transfer channel," *Physical Chemistry Chemical Physics*, vol. 13, no. 8, pp. 3491–3501, 2011.

[14] S. Pavasupree, Y. Suzuki, S. Yoshikawa, and R. Kawahata, "Synthesis of titanate, TiO_2 (B), and anatase TiO_2 nanofibers from natural rutile sand," *Journal of Solid State Chemistry*, vol. 178, no. 10, pp. 3110–3116, 2005.

[15] Y. Q. Gai, J. B. Li, S. S. Li, J. B. Xia, and S. H. Wei, "Design of narrow-gap TiO_2: a passivated codopinga pproach for enhanced photoelectrochemical activity," *Physical Review Letters*, vol. 102, no. 3, Article ID 036402, 4 pages, 2009.

[16] M. L. Chen and W. C. Oh, "The improved photocatalytic properties of methylene blue for V_2O_3/CNT/TiO_2 composite under visible light," *International Journal of Photoenergy*, vol. 2010, Article ID 264831, 5 pages, 2010.

[17] L. Zhao, J. R. Ran, Z. Shu, G. Dai, P. C. Zhai, and S. M. Wang, "Effects of calcination temperatures on photocatalytic activity of ordered titanate nanoribbon/SnO_2 films fabricated during an EPD process," *International Journal of Photoenergy*, vol. 2012, Article ID 472958, 7 pages, 2012.

[18] X. Qin, L. Q. Jing, G. H. Tian, Y. Qu, and Y. Feng, "Enhanced photocatalytic activity for degrading Rhodamine B solution of commercial Degussa P25 TiO_2 and its mechanisms," *Journal of Hazardous Materials*, vol. 172, no. 2-3, pp. 1168–1174, 2009.

[19] C. Deiana, E. Fois, S. Coluccia, and G. Martra, "Surface structure of TiO_2 P25 nanoparticles: infrared study of hydroxy groups on coordinative defect sites," *Journal of Physical Chemistry C*, vol. 114, no. 49, pp. 21531–21538, 2010.

[20] A. I. Kontos, I. M. Arabatzis, D. S. Tsoukleris et al., "Efficient photocatalysts by hydrothermal treatment of TiO_2 ," *Catalysis Today*, vol. 101, no. 3-4, pp. 275–281, 2005.

[21] J. G. Yu and G. H. Wang, "Hydrothermal synthesis and photocatalytic activity of mesoporous titania hollow microspheres," *Journal of Physics and Chemistry of Solids*, vol. 69, no. 5-6, pp. 1147–1151, 2008.

[22] J. G. Yu, H. G. Yu, B. Cheng, M. Zhou, and X. Zhao, "Enhanced photocatalytic activity of TiO_2 powder (P25) by hydrothermal treatment," *Journal of Molecular Catalysis A: Chemical*, vol. 253, no. 1-2, pp. 112–118, 2006.

[23] J. C. Yu, J. Lin, D. Lo, and S. K. Lam, "Influence of thermal treatment on the adsorption of oxygen and photocatalytic activity of TiO_2 ," *Langmuir*, vol. 16, no. 18, pp. 7304–7308, 2000.

[24] S. Sato, T. Kadowaki, and K. Yamaguti, "Photocatalytic oxygen isotopic exchange between oxygen molecule and the lattice oxygen of TiO_2 prepared from titanium hydroxide," *Journal of Physical Chemistry*, vol. 88, no. 14, pp. 2930–2931, 1984.

[25] M. Zhang, Q. Wang, C. C. Chen, L. Zang, W. Ma, and J. Zhao, "Oxygen atom transfer in the photocatalytic oxidation of alcohols by TiO_2: oxygen isotope studies," *Angewandte Chemie—International Edition*, vol. 48, no. 33, pp. 6081–6084, 2009.

[26] K. S. W. Sing, D. H. Everett, R. A. W. Haul et al., "Reporting physisorption data for gas/solid systems with special reference to the determination of surface area and porosity," *Pure and Applied Chemistry*, vol. 57, no. 4, pp. 603–619, 1985.

[27] J. G. Yu, T. T. Ma, G. Liu, and B. Cheng, "Enhanced photocatalytic activity of bimodal mesoporous titania powders by C_{60} modification," *Dalton Transactions*, vol. 40, no. 25, pp. 6635–6644, 2011.

[28] P. Madhusudan, J. R. Ran, J. Zhang, J. Yu, and G. Liu, "Novel urea assisted hydrothermal synthesis of hierarchical $BiVO_4$/$Bi_2O_2CO_3$ nanocomposites with enhanced visible-light photocatalytic activity," *Applied Catalysis B: Environmental*, vol. 110, pp. 286–295, 2011.

[29] J. G. Yu, Y. R. Su, and B. Cheng, "Template-free fabrication and enhanced photocatalytic activity of hierarchical macro-/mesoporous titania," *Advanced Functional Materials*, vol. 17, no. 12, pp. 1984–1990, 2007.

[30] P. Górska, A. Zaleska, E. Kowalska et al., "TiO_2 photoactivity in vis and UV light: the influence of calcination temperature and surface properties," *Applied Catalysis B: Environmental*, vol. 84, no. 3-4, pp. 440–447, 2008.

[31] J. G. Yu, Y. R. Su, B. Cheng, and M. Zhou, "Effects of pH on the microstructures and photocatalytic activity of mesoporous nanocrystalline titania powders prepared via hydrothermal method," *Journal of Molecular Catalysis A: Chemical*, vol. 258, no. 1-2, pp. 104–112, 2006.

[32] J. G. Yu and H. G. Yu, "Facile synthesis and characterization of novel nanocomposites of titanate nanotubes and rutile nanocrystals," *Materials Chemistry and Physics*, vol. 100, no. 2-3, pp. 507–512, 2006.

[33] J. G. Yu, G. H. Wang, B. Cheng, and M. Zhou, "Effects of hydrothermal temperature and time on the photocatalytic activity and microstructures of bimodal mesoporous TiO_2 powders," *Applied Catalysis B: Environmental*, vol. 69, no. 3-4, pp. 171–180, 2007.

[34] P. Du, A. Bueno-López, M. Verbaas et al., "The effect of surface OH-population on the photocatalytic activity of rare earth-doped P25-TiO_2 in methylene blue degradation," *Journal of Catalysis*, vol. 260, no. 1, pp. 75–80, 2008.

[35] Y. H. Ao, J. J. Xu, and D. G. Fu, "Study on the effect of different acids on the structure and photocatalytic activity of mesoporous titania," *Applied Surface Science*, vol. 256, no. 1, pp. 239–245, 2009.

[36] J. G. Yu, M. H. Zhou, B. Cheng, and X. Zhao, "Preparation, characterization and photocatalytic activity of in situ N, S-codoped TiO_2 powders," *Journal of Molecular Catalysis A: Chemical*, vol. 246, no. 1-2, pp. 176–184, 2006.

[37] M. H. Zhou, J. G. Yu, S. W. Liu, P. C. Zhai, and L. Jiang, "Effects of calcination temperatures on photocatalytic activity of SnO_2/TiO_2 composite films prepared by an EPD method," *Journal of Hazardous Materials*, vol. 154, no. 1–3, pp. 1141–1148, 2008.

[38] J. W. Shi, S. H. Chen, S. M. Wang, Z. L. Ye, P. Wu, and B. Xu, "Favorable recycling photocatalyst TiO_2/CFA: effects of calcination temperature on the structural property and photocatalytic activity," *Journal of Molecular Catalysis A: Chemical*, vol. 330, no. 1-2, pp. 41–48, 2010.

[39] K. N. P. Kumar, J. Kumar, and K. Keizer, "Effect of peptization on densification and phase-transformation behavior of sol-gel-derived nanostructured titania," *Journal of the American Ceramic Society*, vol. 77, no. 5, pp. 1396–1400, 1994.

[40] N. Serpone, D. Lawless, and R. Khairutdinov, "Size effects on the photophysical properties of colloidal anatase TiO_2 particles: size quantization versus direct transitions in this indirect semiconductor?" *Journal of Physical Chemistry*, vol. 99, no. 45, pp. 16646–16654, 1995.

[41] H. G. Yu, J. G. Yu, B. Cheng, and M. Zhou, "Effects of hydrothermal post-treatment on microstructures and morphology of titanate nanoribbons," *Journal of Solid State Chemistry*, vol. 179, no. 2, pp. 349–354, 2006.

[42] Q. Xiao and L. L. Ouyang, "Photocatalytic activity and hydroxyl radical formation of carbon-doped TiO_2 nanocrystalline: effect of calcination temperature," *Chemical Engineering Journal*, vol. 148, no. 2-3, pp. 248–253, 2009.

[43] J. G. Yu and J. G. Ran, "Facile preparation and enhanced photocatalytic H_2-production activity of $Cu(OH)_2$ cluster modified TiO_2 ," *Energy & Environmental Science*, vol. 4, no. 4, pp. 1364–1371, 2011.

[44] C. C. Tsai and H. Teng, "Regulation of the physical characteristics of titania nanotube aggregates synthesized from hydrothermal treatment," *Chemistry of Materials*, vol. 16, no. 22, pp. 4352–4358, 2004.

[45] J. G. Yu, J. C. Yu, M. K. P. Leung et al., "Effects of acidic and basic hydrolysis catalysts on the photocatalytic activity and microstructures of bimodal mesoporous titania," *Journal of Catalysis*, vol. 217, no. 1, pp. 69–78, 2003.

[46] Q. J. Xiang, K. L. Lv, and J. G. Yu, "Pivotal role of fluorine in enhanced photocatalytic activity of anatase TiO_2 nanosheets with dominant (001) facets for the photocatalytic degradation of acetone in air," *Applied Catalysis B: Environmental*, vol. 96, no. 3-4, pp. 557–564, 2010.

[47] S. W. Liu, J. G. Yu, and M. Jaroniec, "Tunable photocatalytic selectivity of hollow TiO_2 microspheres composed of anatase polyhedra with exposed {001} facets," *Journal of the American Chemical Society*, vol. 132, no. 34, pp. 11914–11916, 2010.

[48] D. C. Hurum, A. G. Agrios, K. A. Gray, T. Rajh, and M. C. Thurnauer, "Explaining the enhanced photocatalytic activity of Degussa P25 mixed-phase TiO_2 using EPR," *Journal of Physical Chemistry B*, vol. 107, no. 19, pp. 4545–4549, 2003.

[49] J. G. Yu, L. J. Zhang, B. Cheng, and Y. Su, "Hydrothermal preparation and photocatalytic activity of hierarchically sponge-like macro-/mesoporous titania," *Journal of Physical Chemistry C*, vol. 111, no. 28, pp. 10582–10589, 2007.

[50] N. R. C. Fernandes Machado and V. S. Santana, "Influence of thermal treatment on the structure and photocatalytic activity of TiO_2 P25," *Catalysis Today*, vol. 107-108, pp. 595–601, 2005.

[51] R. R. Bacsa and J. Kiwi, "Effect of rutile phase on the photocatalytic properties of nanocrystalline titania during the degradation of p-coumaric acid," *Applied Catalysis B: Environmental*, vol. 16, no. 1, pp. 19–29, 1998.

[52] S. Bakardjieva, J. Šubrt, V. Štengl, M. J. Dianez, and M. J. Sayagues, "Photoactivity of anatase-rutile TiO_2 nanocrystalline mixtures obtained by heat treatment of homogeneously precipitated anatase," *Applied Catalysis B: Environmental*, vol. 58, no. 3-4, pp. 193–202, 2005.

[53] J. G. Yu and B. Wang, "Effect of calcination temperature on morphology and photoelectrochemical properties of anodized titanium dioxide nanotube arrays," *Applied Catalysis B: Environmental*, vol. 94, no. 3-4, pp. 295–302, 2010.

[54] K. L. Lv, Q. J. Xiang, and J. G. Yu, "Effect of calcination temperature on morphology and photocatalytic activity of anatase TiO_2 nanosheets with exposed {001} facets," *Applied Catalysis B: Environmental*, vol. 104, no. 3-4, pp. 275–281, 2011.